nature portfolio

https://doi.org/10.1038/s41561-022-01024-y

## Supplementary information

# Hydrous peridotitic fragments of Earth's mantle 660 km discontinuity sampled by a diamond

In the format provided by the authors and unedited

# Hydrous peridotitic fragments of Earth's mantle 660 km discontinuity sampled by a diamond

**[1,2]Tingting Gu*, [3]Martha G. Pamato, [3]Davide Novella, [4]Matteo Alvaro, [5]John Fournelle, [6]Frank E. Brenker,[1]Wuyi Wang, [3,6]Fabrizio Nestola***

[1]Gemological Institute of America, New York, NY 10036, USA
[2]The Department of Earth, Atmospheric, and Planetary Sciences, Purdue University, West Lafayette, IN, 47907, USA
[3]Department of Geosciences, University of Padova, 35131 Padova, Italy
[4]Department of Earth and Environmental Sciences, University of Pavia, 27100 Pavia, Italy
[5]Department of Geoscience, University of Wisconsin, Madison, WI, 53706, USA
[6]Department of Geoscience, Goethe University Frankfurt, 60438 Frankfurt am Main, Germany

* corresponding authors

**List of Supplementary Materials:**

**Supplementary Figs** 1-5

**Supplementary Tables** 1-5

**Supplementary Databases** 1-14

**Supplementary Figs** 1-5

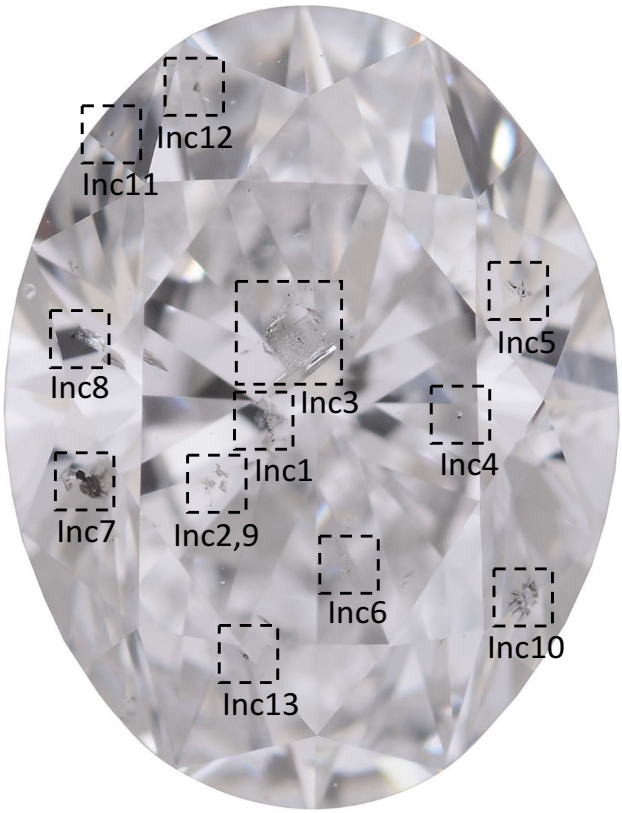


**Supplementary Fig. 1** A layout of all the inclusions observed in the 1.5 ct. diamond. The diamond is 8.49 mm along its longest dimension.

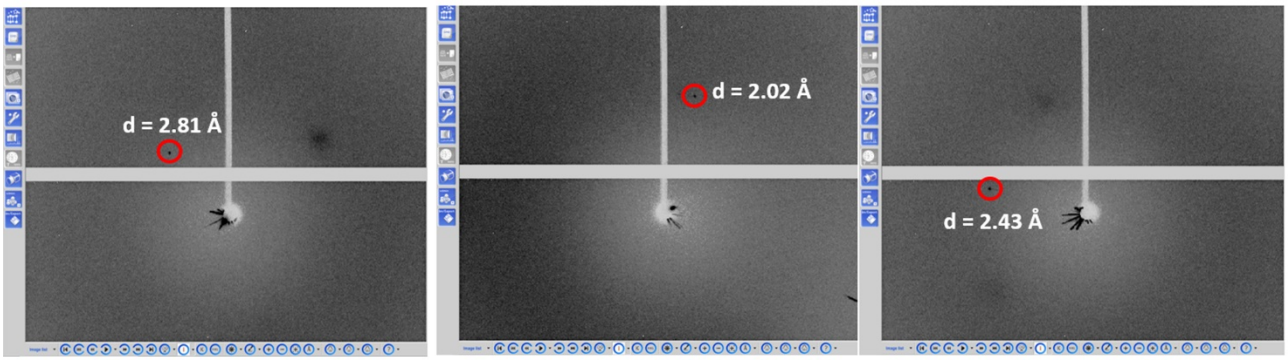


**Supplementary Fig. 2** X-ray diffraction images collected on inclusion 5. The reflections circled in red represents the *d* spacing of 2.81, 2.02 and 2.43 Å. These sharp reflections possibly do not overlap with diamond, ferropericlase, or enstatite and could confidently be assigned to ringwoodite. In fact, enstatite does not have any significant intense reflection at 2.02 Å and ferropericlase, with composition $Mg_{0.9}Fe_{0.1}O$, has its main reflection well shifted with respect to 2.02 at 2.11 Å. In addition, ferropericlase inclusions in diamonds usually show very broad diffraction reflections [5,41]. Finally, we can exclude that this reflection belongs to the diamond host as not only diamond has its main peak at 2.06 Å but also reflections from such a huge diamond are extremely broad and spread over several pixels in one single diffraction image.

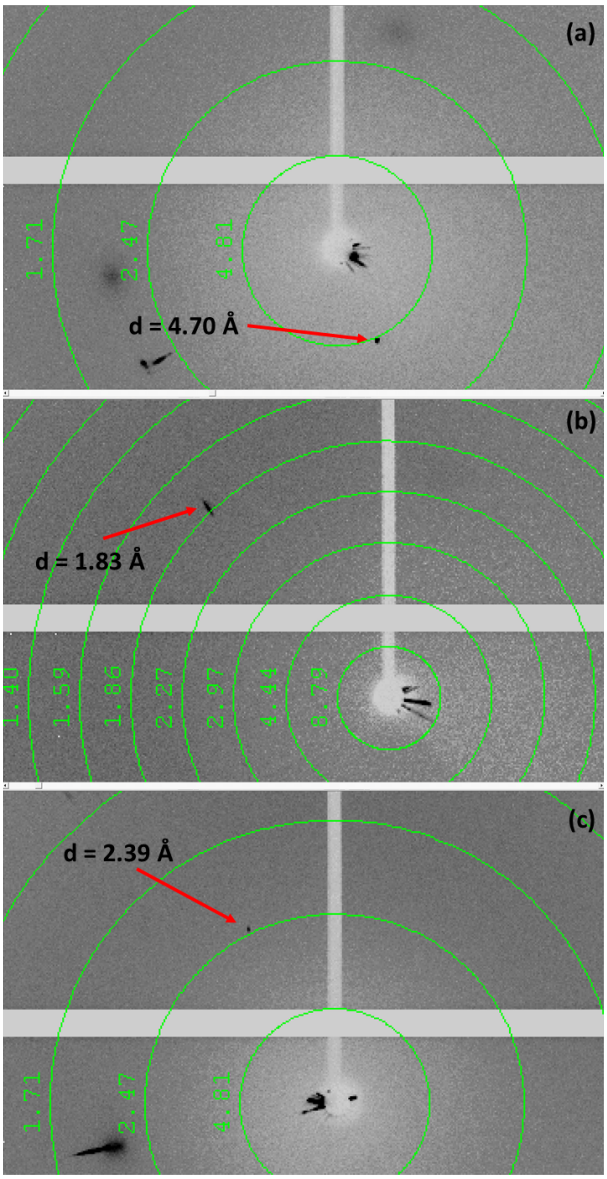


**Supplementary Fig. 3** Diffraction spots collected on inclusion 5 that could be assigned to brucite. In detail, in (a) the diffraction spot at 4.70 Å can be only assigned to brucite as such *d* spacing is not present in ferropericlase, ringwoodite or enstatite. The same applies for the diffraction spot in (b) at 1.83 Å. These two represent the second and the third most intense peaks of brucite, respectively. The diffraction spot in (c) at 2.39 Å, which corresponds to the most intense peak of brucite, cannot be unequivocally assigned to brucite as it can also be assigned to ferropericlase and ringwoodite (showing peaks at 2.45 and 2.43 Å, respectively). Enstatite has also a very intense peak at 2.49 Å, but it is too far in *d* spacing with respect to 2.39 Å. It is very likely, however, that the peak at 2.39 Å does not belong to ferropericlase because of its low intensity: in ferropericlase the peak at 2.45 Å is quite intense being the third most intense peak. Ringwoodite has the strongest reflection at 2.43 Å. In this case we cannot discriminate, based purely on the intensity, given the small size of the ringwoodite inclusion. However, considering the two peaks at 4.70 and 1.83 Å, we cannot exclude that the peak at 2.39 Å also belongs to brucite.

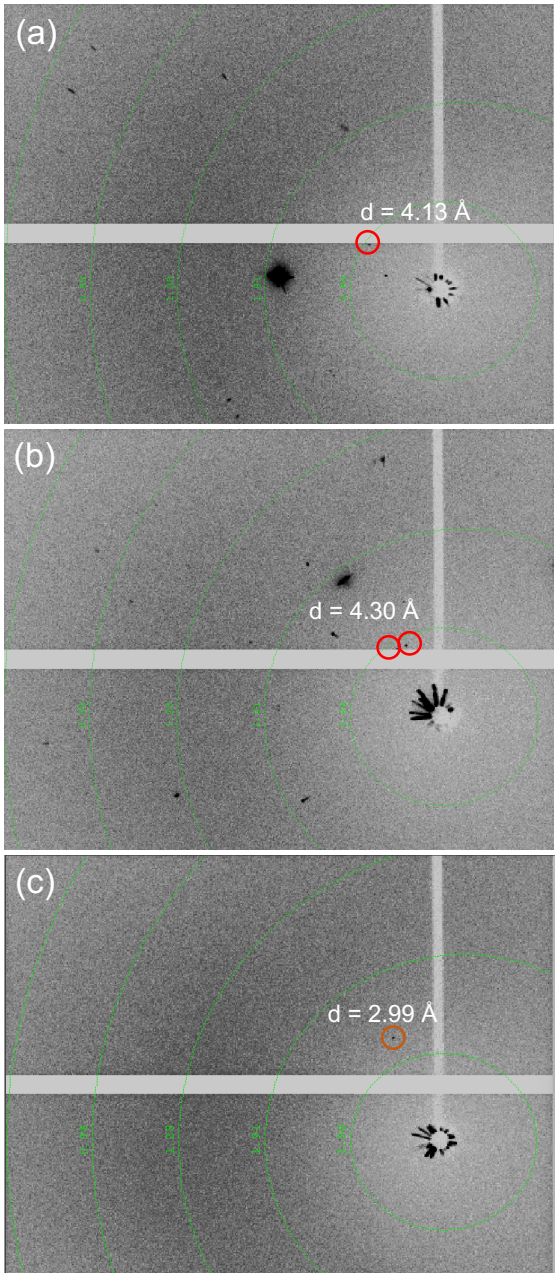


**Supplementary Fig. 4** X-ray diffraction spots collected on inclusion 2c that could be assigned to phase D. In detail, in (a) the diffraction spot at 4.13 Å can be only assigned to phase D at (100) as such *d* spacing is not present in ferropericlase, ringwoodite, olivine or enstatite. The same applies for the two diffraction spots in (b) at 4.30 Å that could be assigned to phase D at (001). The diffraction spot in (c) at 2.99 Å, which corresponds to the most intense peak of phase D[75], cannot be unequivocally assigned to phase D as it could be assigned to the (220) reflection from magnesioferrite at ~2.95 Å, possibly an exsolution from ferropericlase. However, considering the internal pressure of these inclusions, which could be ~1.3 GPa, the reflection of magnesioferrite at (220) could shift to ~2.92 Å that might be much smaller in *d* spacing with respect to the peak observed here at 2.99 Å. Considering the peaks at 4.13 and 4.30 Å, as well as the Raman spectra, we cannot exclude that the peak at 2.99 Å also belongs to phase D.

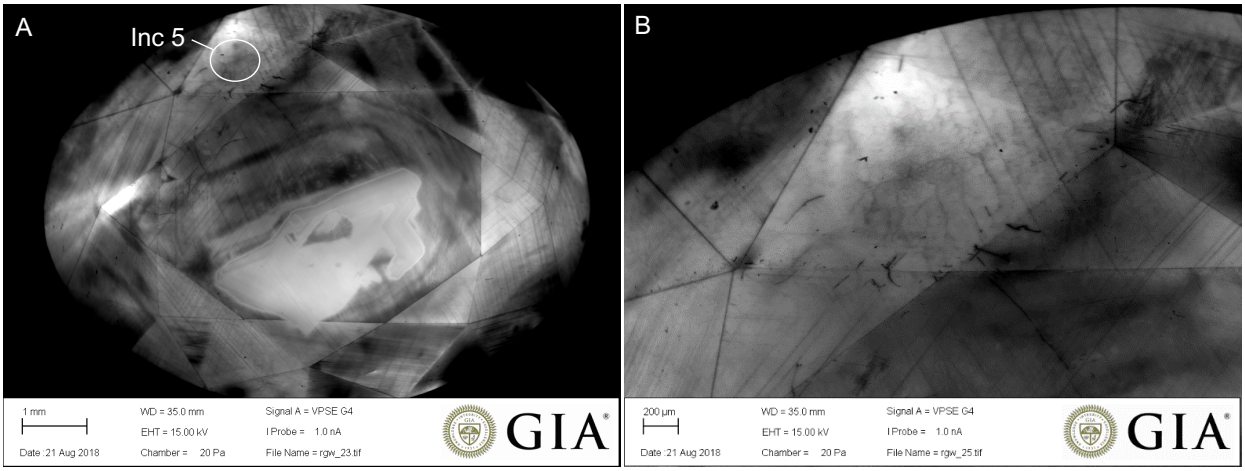


**Supplementary Fig. 5** Cathodoluminescence image taken by Zeiss EVO 25 SEM under low vacuum mode, 15 kV, 1.0 nA, and 35.0 mm working distance for the whole diamond (A) and the area around inclusion 5 (B).

**Supplementary Tables 1-5**

**Supplementary Table 1.** Mineral phases detected by micro-Raman spectroscopy, single-crystal X-ray diffraction and EMPA within the 1.5 ct. diamond investigated in this work.

| Inclusion | Phases | Method |
|---|---|---|
| Inc 1a | Enstatite | Raman, XRD |
| Inc 1b | Enstatite; ringwoodite | Raman & XRD; Raman & EMPA |
| Inc 1c | Enstatite | Raman, XRD, EMPA |
| Inc 2a | Enstatite; ringwoodite | Raman & XRD; Raman |
| Inc 2b | Enstatite, olivine | Raman & XRD |
| Inc 2c | Enstatite, phase D*; coesite, olivine/ringwoodite, ferropericlase; | Raman & XRD; Raman |
| Inc 4 | Enstatite, olivine; perovskite-type mineral* | Raman & XRD; Raman |
| Inc 5 | Enstatite, ringwoodite, brucite*; ferropericlase | Raman & XRD; XRD |
| Inc 5b | Enstatite, olivine, magnesite | Raman |
| Inc 6 | Enstatite | Raman & XRD |
| Inc 8 | Enstatite | Raman & XRD |
| Inc 9 | Ferropericlase (with exsolution of Mg-Fe spinel) | Raman & XRD |
| Inc 10 | Ferropericlase | XRD |
| Inc 11 | Ferropericlase | XRD, EMPA |

*Possible identification based on the available Raman and XRD data.

**Supplementary Table 2.** Unit-cell parameters of the inclusions within the 1.5 ct. diamond measured by single-crystal X-ray diffraction. *Based on the size of the inclusions, we refine the cell parameters using between 100 and 1000 reflections.

| **Inclusions** | **phase** | ***a* (Å)** | ***b* (Å)** | ***c* (Å)** | ***V* (Å$^3$)** |
|---|---|---|---|---|---|
| Inc 1a | Enstatite | 18.12(10) | 8.79(6) | 5.18(3) | 825(1) |
| Inc 1b | Enstatite | 18.19(2) | 8.791(6) | 5.178(5) | 828.0(6) |
| Inc 1c | Enstatite | 18.190(1) | 8.777(1) | 5.177(5) | 826(1) |
| Inc 2a | Enstatite | 18.10(7) | 8.786(7) | 5.168(4) | 822(1) |
| Inc 2b | Enstatite | 18.109(8) | 8.774(5) | 5.210(4) | 827(1) |
| Inc 2c | Enstatite | 18.185(7) | 8.804(4) | 5.172(6) | 828.1(8) |
| Inc 4 | Enstatite | 18.186(5) | 8.78(6) | 5.178(5) | 826.8(9) |
| Inc 5 | Enstatite | 18.154(9) | 8.776(5) | 5.179(4) | 825.1(8) |
| Inc 5 | Ferropericlase | 4.221(7) | 4.221(7) | 4.221(7) | 75.2(2) |
| Inc 6 | Enstatite | 18.18(1) | 8.776(4) | 5.173(5) | 825.3(8) |
| Inc 8 | Enstatite | 18.10(2) | 8.763(8) | 5.208(6) | 826.1(9) |
| Inc 10 | Ferropericlase | 4.186(1) | 4.186(1) | 4.186(1) | 73.36(5) |

**Supplementary Table 3.** Microprobe analyses performed on two larger ringwoodite grains close to inclusion 1b in Figure 1c. *measured under 15 kV; and the data without marks were measured at 10 kV. (See Methods for the description of the instrumentation and the experimental setup). Ca, Cr, Ni are below detection level.

| **Oxide (wt%)** | grain 1 | grain 1* | grain 2 | **Average** |
|---|---|---|---|---|
| MgO | 50.05 | 49.55 | 50.20 | 49.93 |
| $SiO_2$ | 40.54 | 38.66 | 40.51 | 39.90 |
| FeO | 7.54 | 7.47 | 7.44 | 7.48 |
| MnO | 0.33 | 0.14 | 0.20 | 0.22 |
| Total | 98.47 | 95.82 | 98.25 | 97.51 |
| Mg# | 92.2 | 92.3 | 92.4 | 92.3 |

**Supplementary Table 4.** Microprobe analyses performed on enstatite of inclusion 1b and 1c (see the Methods for the description of the instrumentation and the experimental setup). El. = Element; BDL = below detection level.

| **Oxide** | **Inc 1b (*wt %*)** | ***n. of spots*** | **Inc 1c (*wt %*)** | ***n. of spots*** | ***Average*** | **El.** | ***El wt%*** | ***Standard deviation*** | **Standard** |
|---|---|---|---|---|---|---|---|---|---|
| $Na_2O$ | 0.06 | 24 | 0.06 | 9 | 0.06 | Na | 0.05 | 16% | Jadeite |
| MgO | 36.13 | 24 | 36.07 | 9 | 36.12 | Mg | 21.78 | 1.2% | Syn. Enstatite |
| $Al_2O_3$ | 1.18 | 24 | 1.19 | 9 | 1.18 | Al | 0.63 | 2.7% | Jadeite |
| $SiO_2$ | 56.51 | 24 | 56.97 | 9 | 56.64 | Si | 26.47 | 1.1% | Syn. Enstatite |
| CaO | 0.02 | 24 | 0.02 | 9 | 0.02 | Ca | 0.01 | 27% | Augite |
| $TiO_2$ | 0.20 | 24 | 0.19 | 9 | 0.19 | Ti | 0.12 | 7.7% | Syn. $TiO_2$ |
| FeO | 4.67 | 24 | 4.69 | 9 | 4.68 | Fe | 3.64 | 3.6% | Hematite |
| MnO | 0.23 | 24 | 0.23 | 9 | 0.28 | Mn | 0.17 | 18% | Tephroite |
| $V_2O_3$ | BDL | 24 | BDL | 9 | BDL | V | BDL | | V metal |
| $Cr_2O_3$ | 0.31 | 24 | 0.31 | 9 | 0.31 | Cr | 0.21 | 13% | Syn. $Cr_2O_3$ |
| NiO | BDL | 24 | BDL | 9 | BDL | Ni | BDL | | Ni metal |
| | | | | | | O | 46.35 | | |
| Total | 99.29 | | 99.75 | | 99.45 | | 99.45 | | |
| Mg# | 93.3 | | 93.3 | | 93.3 | | | | |

**Supplementary Table 5.** Microprobe analyses performed on ferropericlase of inclusion 11 (see Methods for the description of the instrumentation and the experimental setup). CaO, $K_2O$ and $TiO_2$ were below the instrumental detection limit.

| **Oxide** | ***Wt %*** | ***Standard deviation*** | ***n. of spots*** |
|---|---|---|---|
| MgO | 73.56 | 0.74 | 21 |
| FeO | 24.22 | 0.29 | 24 |
| NiO | 1.73 | 0.09 | 24 |
| $Cr_2O_3$ | 0.48 | 0.03 | 24 |
| $Na_2O$ | 0.23 | 0.05 | 15 |
| MnO | 0.17 | 0.02 | 15 |
| $Al_2O_3$ | 0.04 | 0.02 | 15 |
| $SiO_2$ | 0.04 | 0.03 | 15 |
| Total | 100.47 | | |
| Mg# | 84.5 | | |

**Supplementary Databases: 1-14** mineral inclusions identified by Raman in the 1.5 ct. diamond.

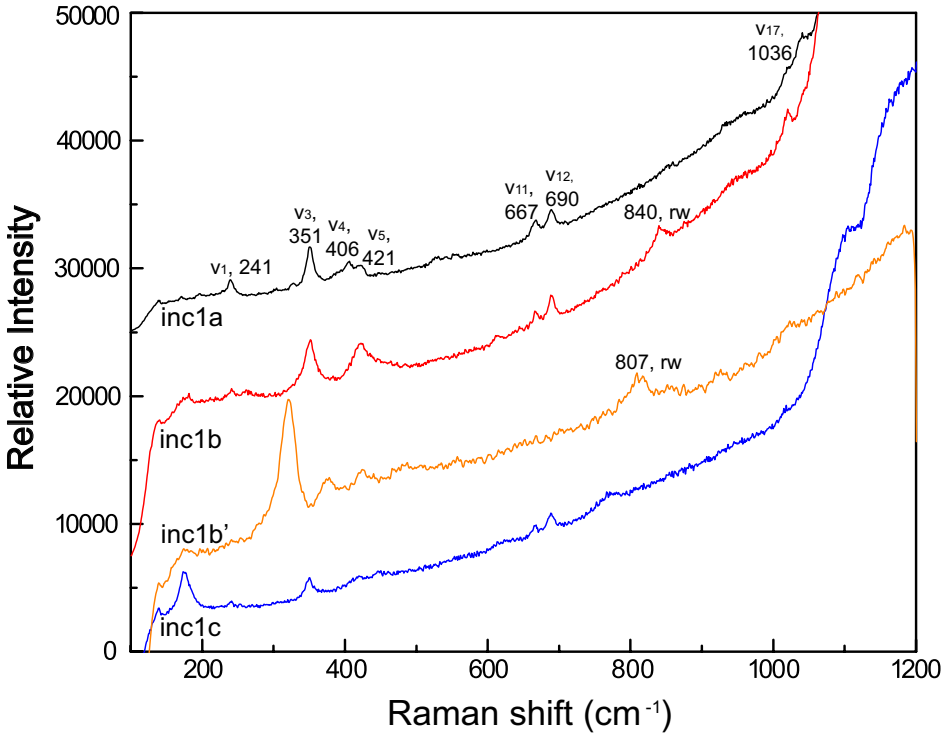


**Supplementary Database 1:** Raman spectra collected at GIA of inclusion 1a, 1b, 1b′ and 1c. The spectrum of inclusion inc1a in black is assigned to enstatite, whereas the spectrum in red, together with enstatite, also shows a peak at ~840 $cm^{-1}$ that can be attributed to ringwoodite (rw). This spectrum was collected when the inclusion was imbedded in the diamond. The spectrum of inc1b′ was collected at the micrometric sized inclusion with its tip exposed to the surface after polishing (the larger one at the centre in Figure 1c) and again shows low-intensity enstatite peaks in addition to the potential ringwoodite doublet (evident peak at 807 $cm^{-1}$). We were not able to assign the intense peak at about 320 $cm^{-1}$ in the yellow spectrum of inclusion inc1b′.

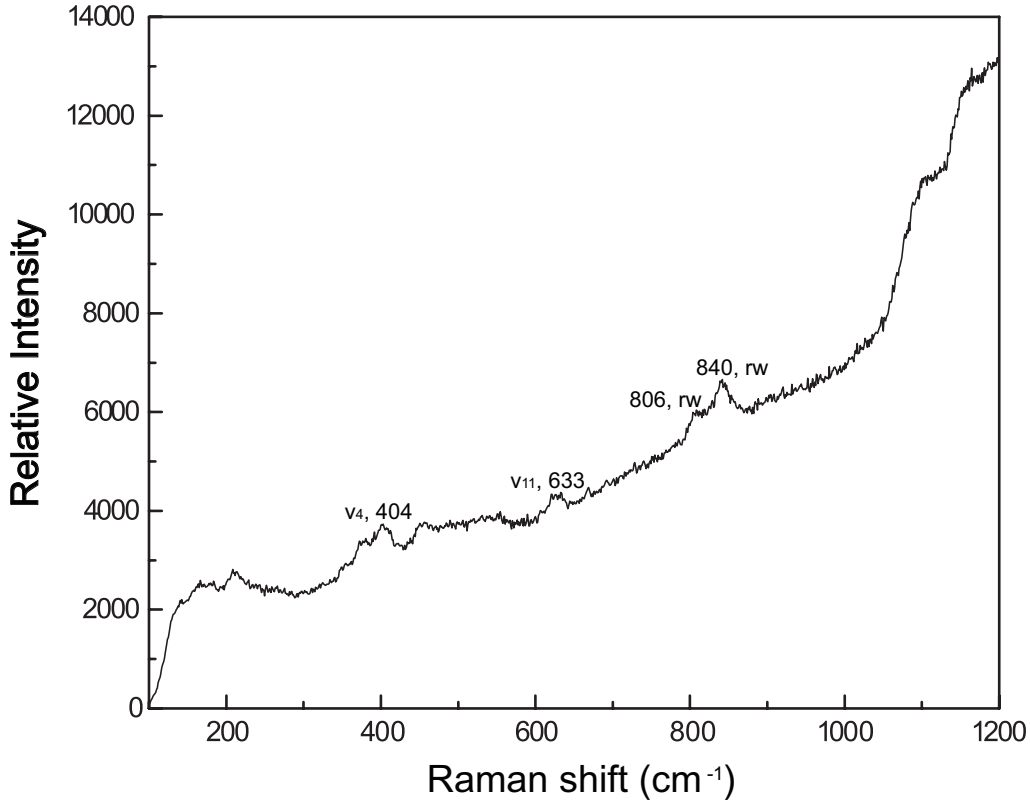


**Supplementary Database 2:** Raman spectrum collected at GIA for inclusion 2a. Ringwoodite peaks are marked by "rw", while the other peaks are assigned to enstatite.

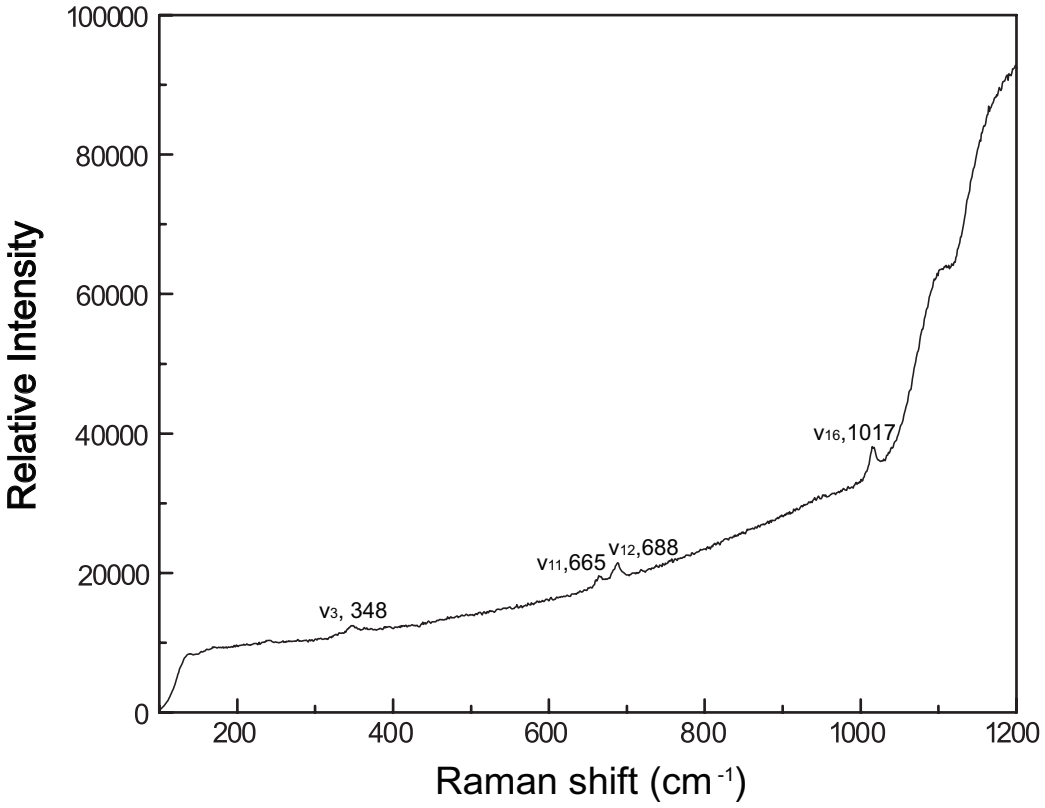


**Supplementary Database 3:** Raman spectrum collected at GIA for inclusion 2b, with all peaks assigned to enstatite.

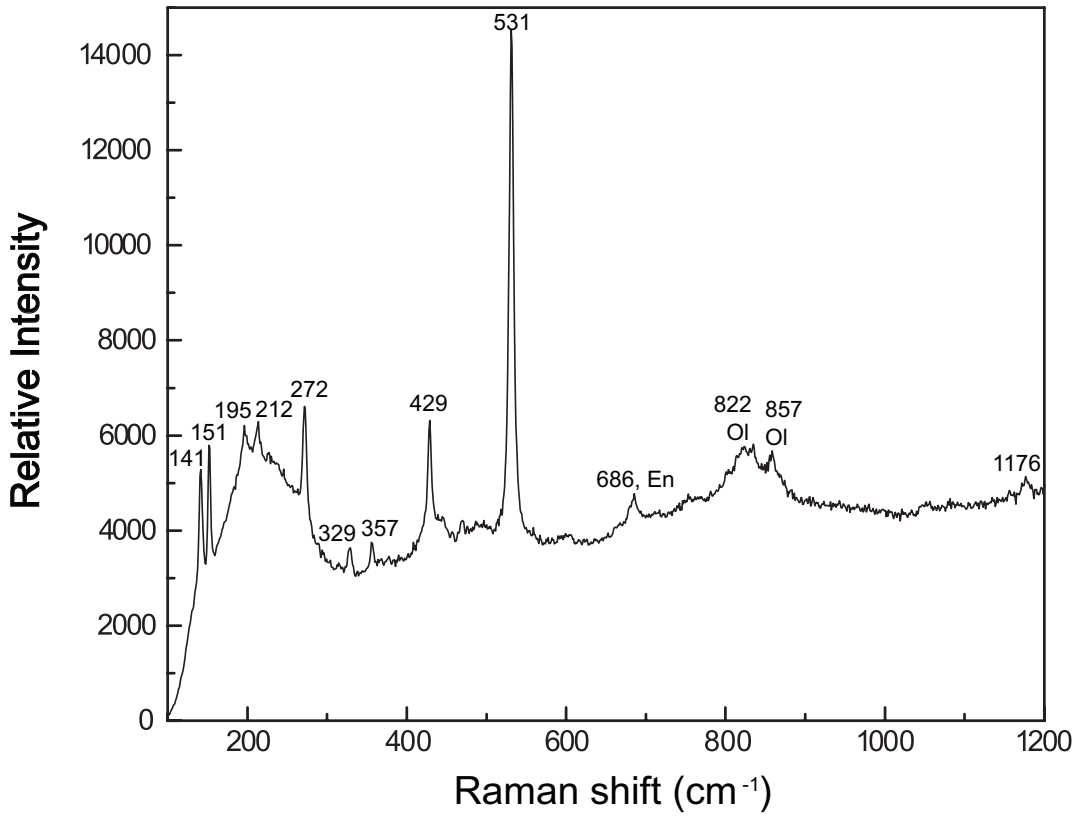


136

137 **Supplementary Database 4**: Raman spectrum collected at GIA for an additional area of inclusion
138 2c, with the listed peak positions assigned to coesite, except for one peak at 686 $cm^{-1}$ assigned to
139 enstatite ($\nu_{12}$). The bump around 200 $cm^{-1}$ could be caused by the coexisting ferropericlase. Two
140 peaks at 822 and 857 $cm^{-1}$ are assigned to olivine as a back transformation from ringwoodite.

141

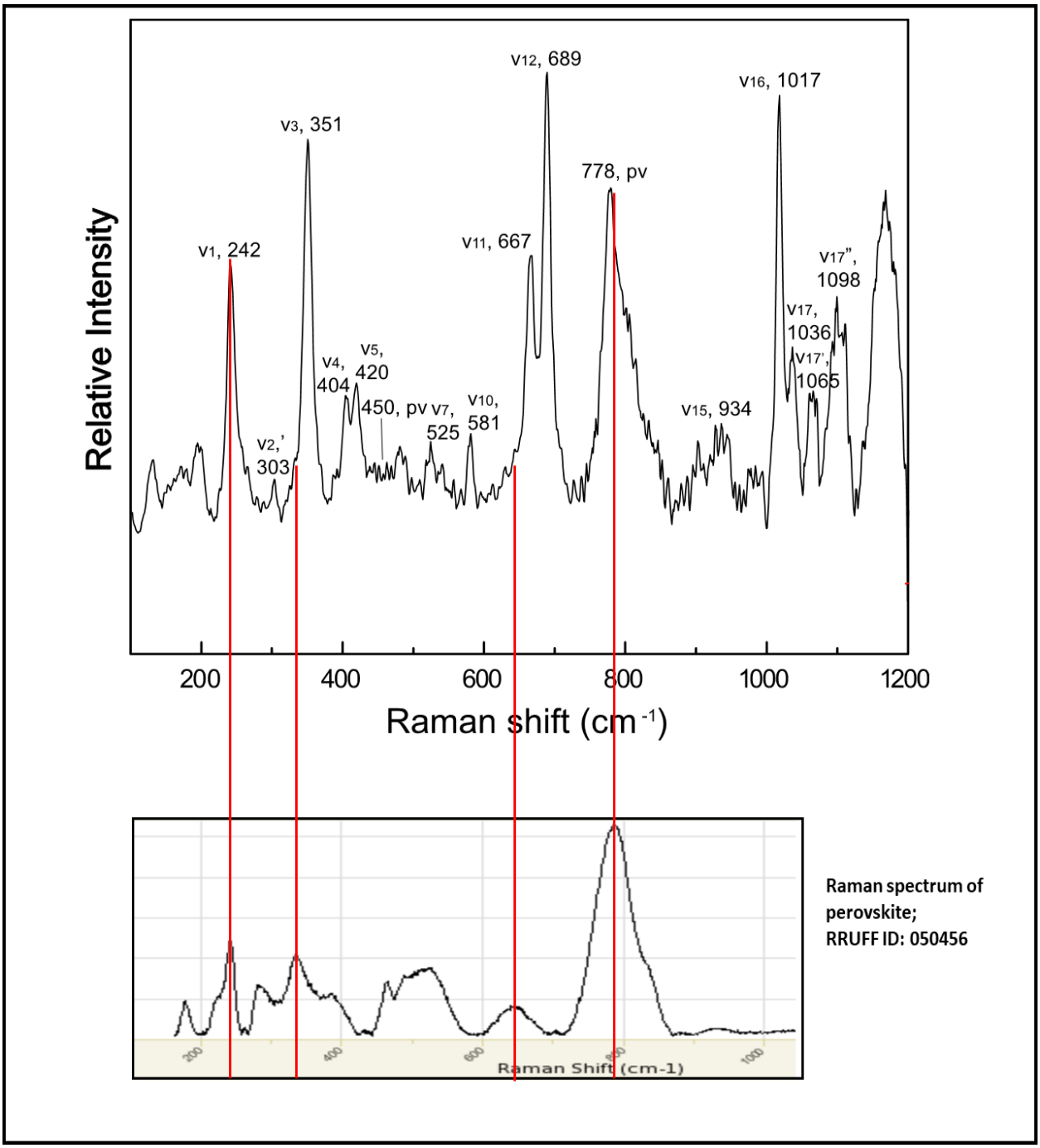


142

143 **Supplementary Database 5**: Raman spectrum collected at GIA for inclusion 4. Most of the peaks
144 belong to enstatite, whereas the remaining peaks were assigned to a perovskite-type mineral. The
145 reference Raman spectrum of perovskite (RRUFF ID R050456) is reported on the bottom (the red
146 lines are guides to the eye and are used for comparison).

147

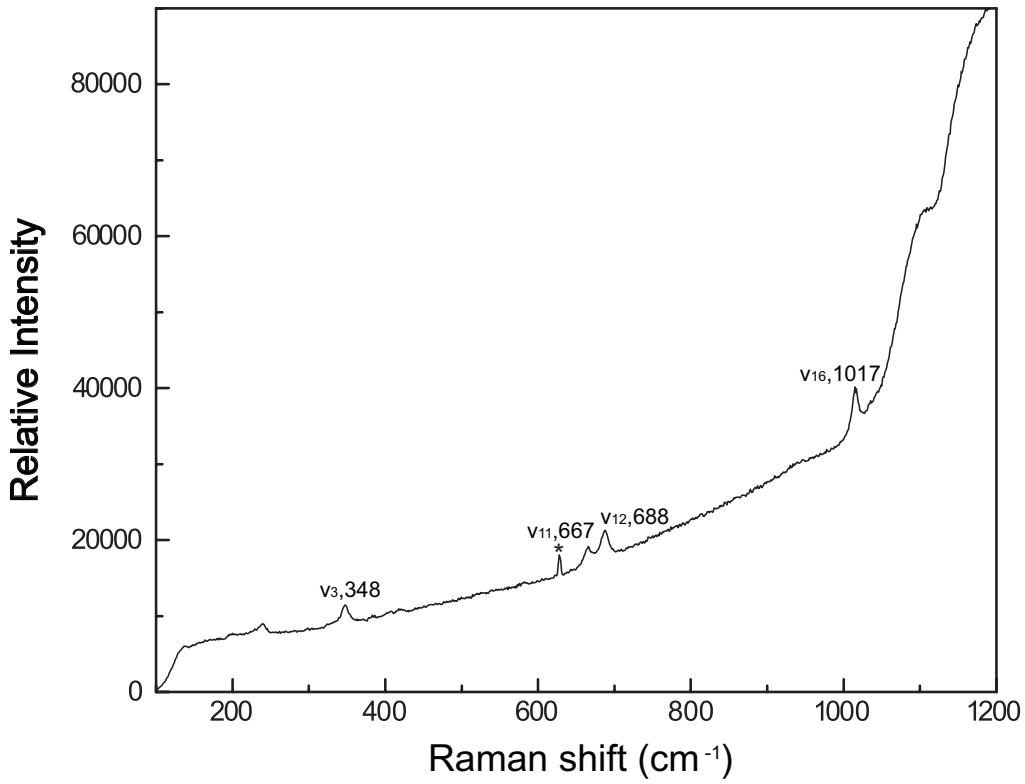


**Supplementary Database 6**: Raman spectrum collected at GIA for inclusion 6. Peak positions listed here are assigned to enstatite. Unknown peak at 628 $cm^{-1}$ is marked with "*".

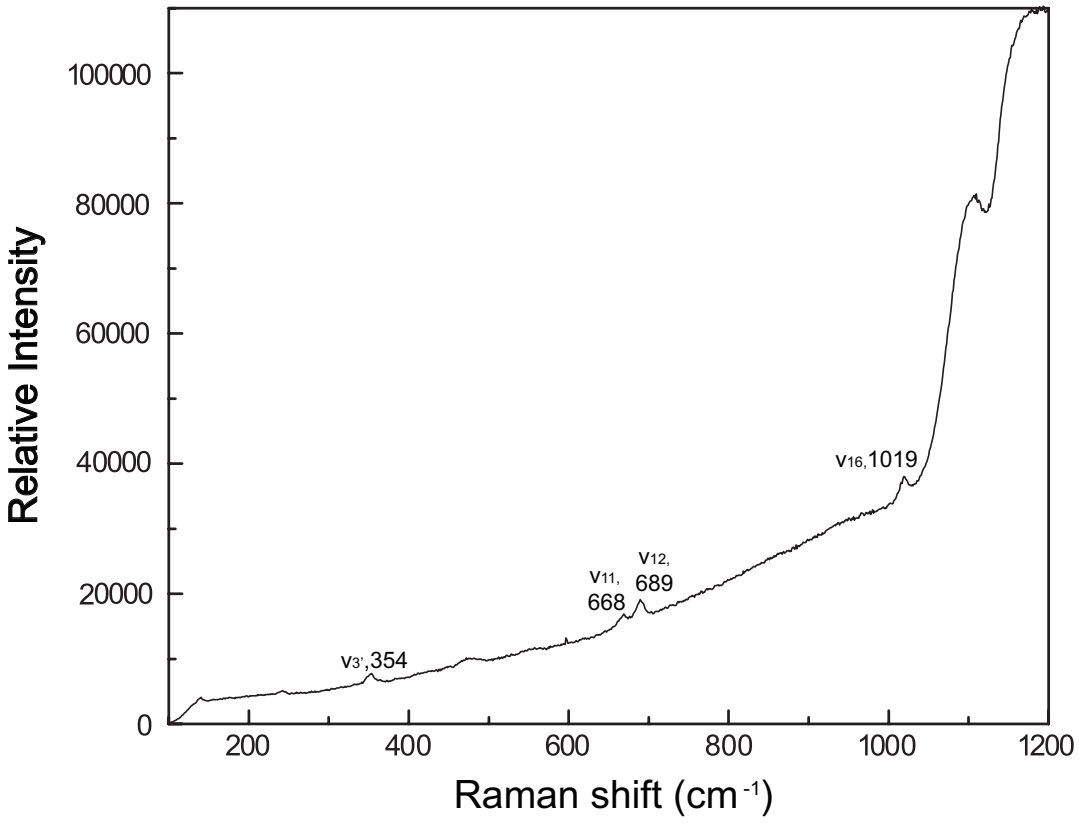


**Supplementary Database 7**: Raman spectrum collected at GIA for inclusion 8, which is identified as enstatite. Raman bands are located at 354, 668, 689 $cm^{-1}$, which are slightly shifted with respect inclusions 1 and 2, possibly due to higher residual pressure (assuming that all enstatite in the same diamond have a similar composition).

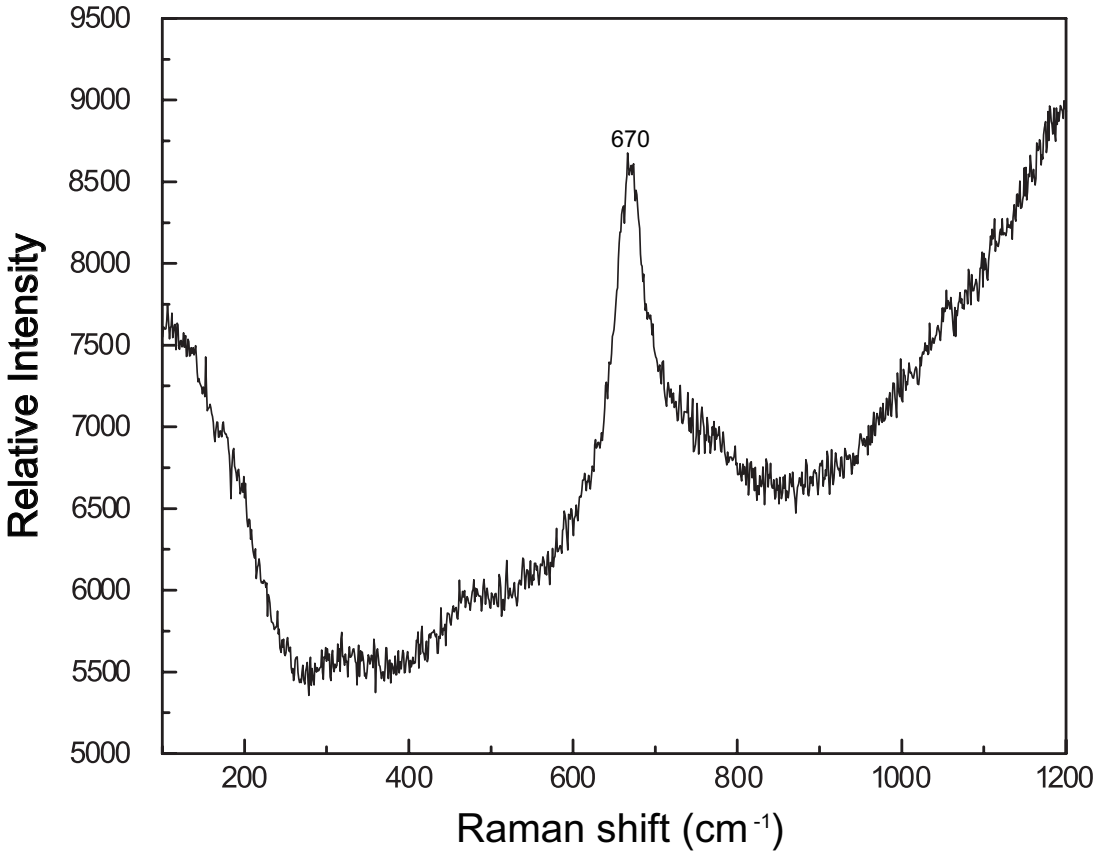


157

158 **Supplementary Database 8**: Raman spectrum collected at GIA for inclusion 9, which is
159 positioned within the diamond and is close to inclusion 2. The broad peak at 670 $cm^{-1}$ is typical of
160 the spinel series magnetite-magnesioferrite. This spinel phase is typically found as exsolutions in
161 ferropericlase [5,41] and in average such exsolved phase represents about 6-7% of the ferropericlase
162 grains.

163

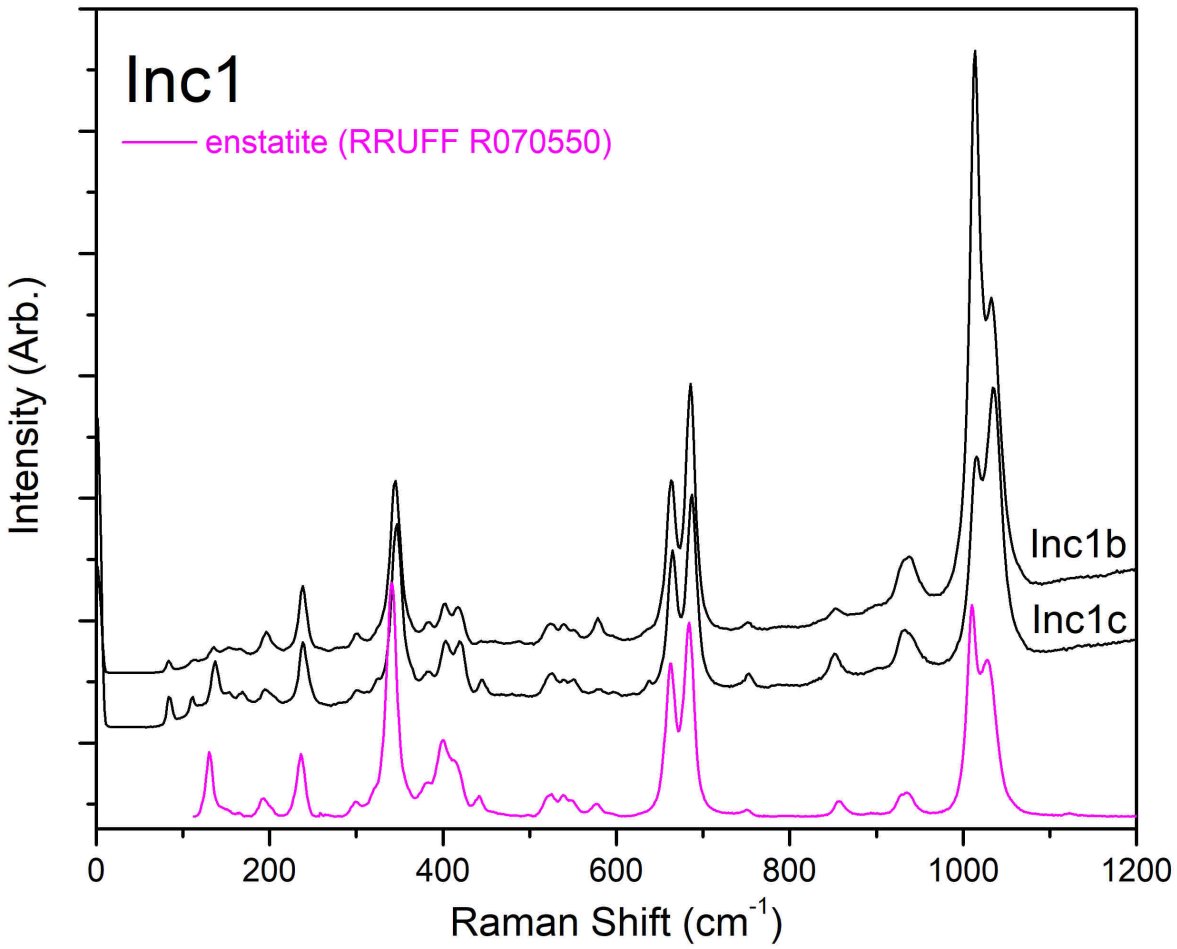


164

165 **Supplementary Database 9**: Raman spectra collected at Northwestern University on inclusion 1b
166 and 1c showing enstatite.

167

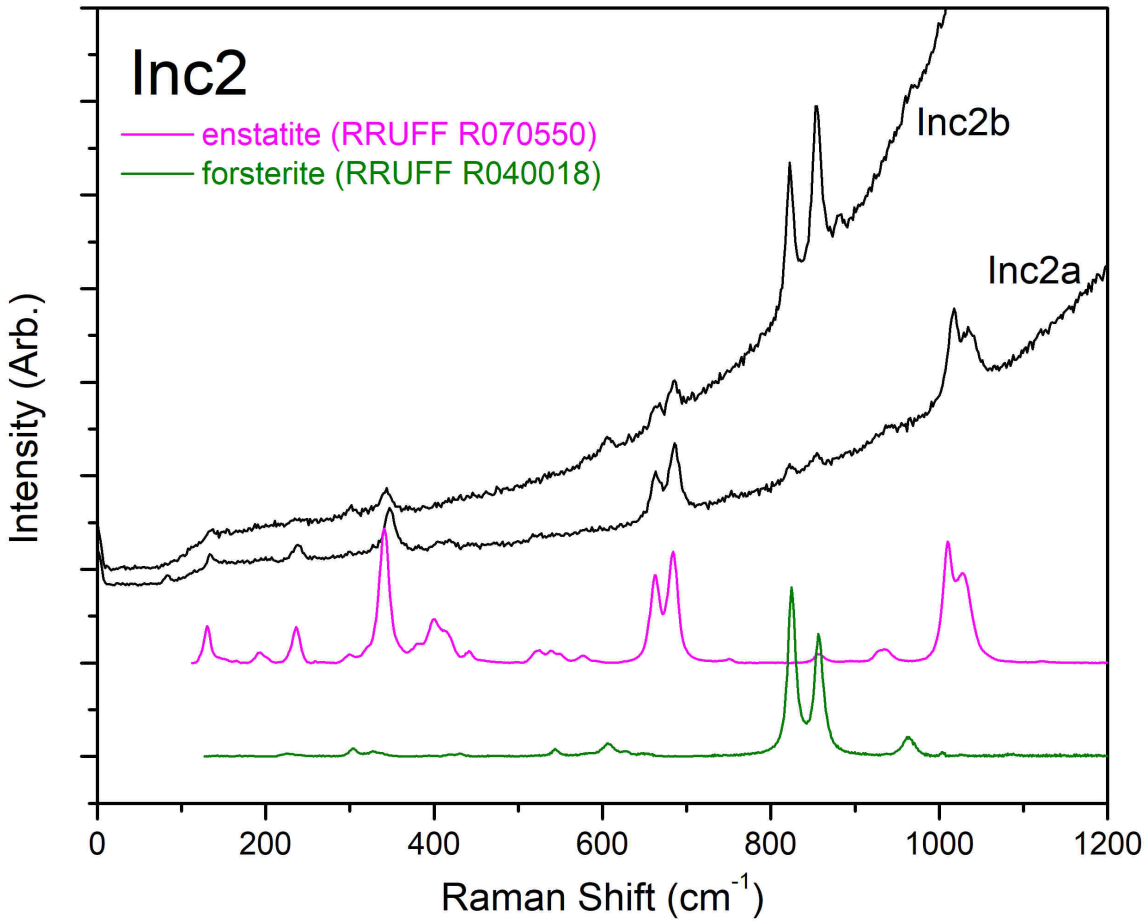


168

169 **Supplementary Database 10**: Raman spectra collected at Northwestern University on inclusion
170 2a and 2b showing a mixture of olivine and enstatite.

171

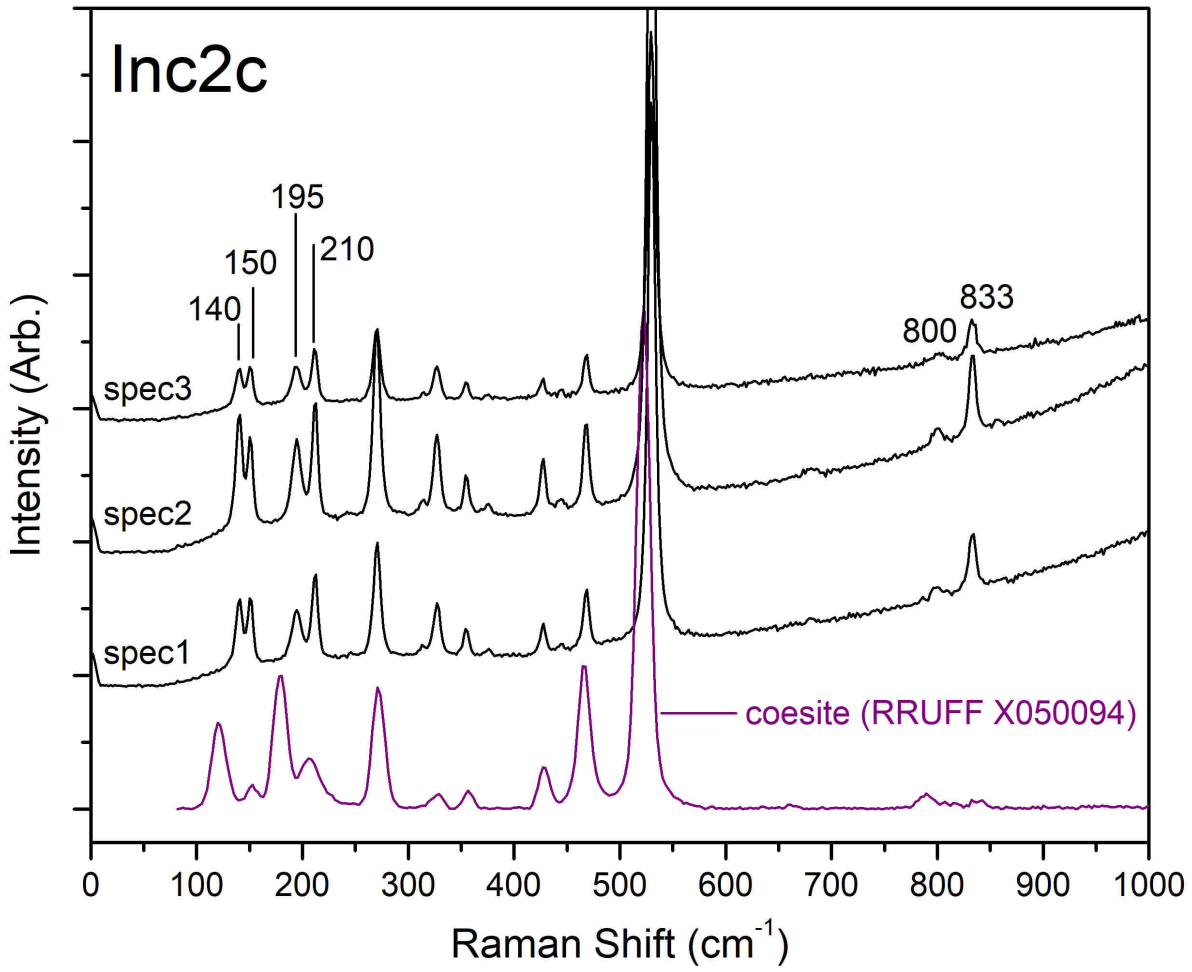


172

173 **Supplementary Database 11**: Raman spectra collected at Northwestern University on inclusion
174 2c showing coesite. Peaks labeled 800 and 833 $cm^{-1}$ are likely associated with ringwoodite or
175 partially reverted ringwoodite to olivine.

176

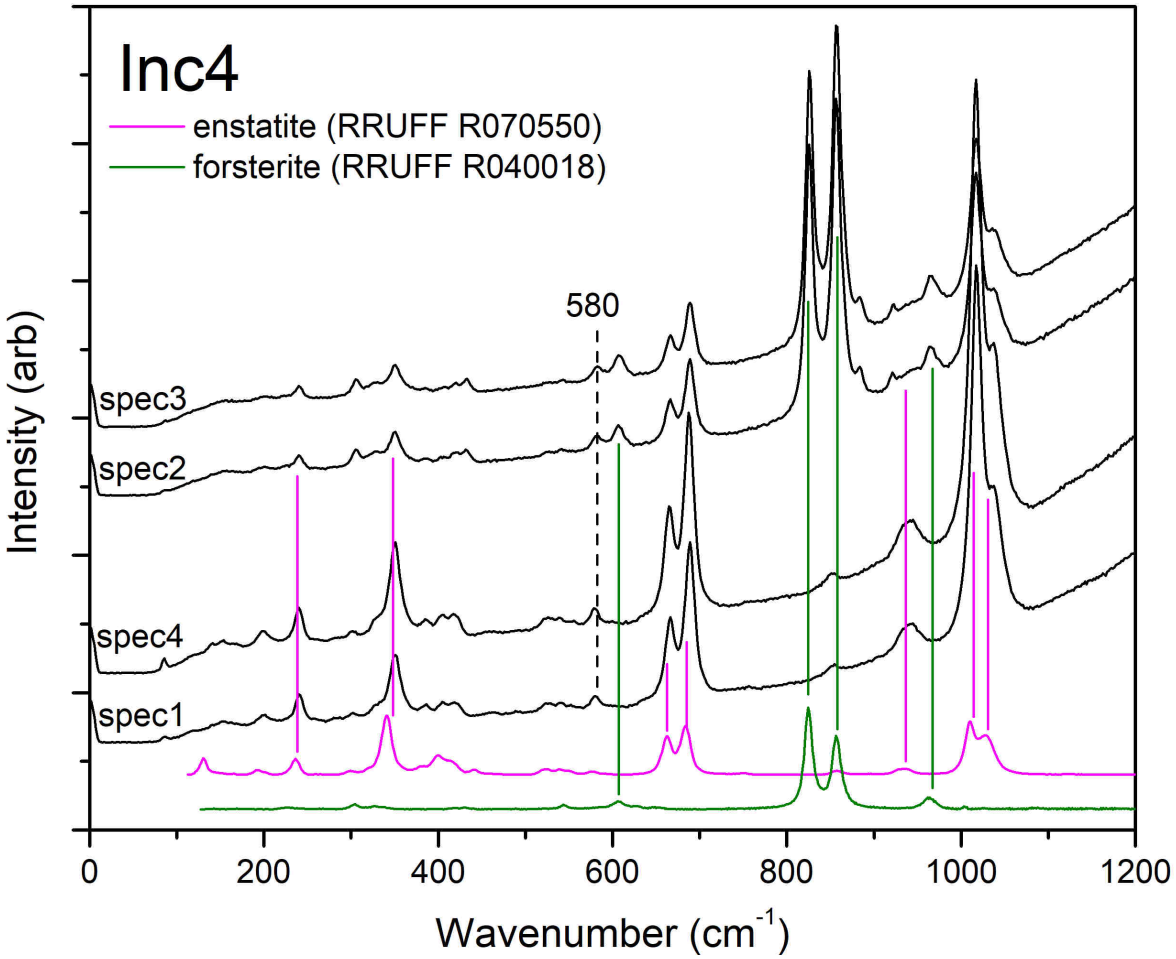


177

178 **Supplementary Database 12**: Raman spectra collected at Northwestern University on inclusion
179 4 showing a mixture of enstatite and forsterite. Only the band at 580 $cm^{-1}$ could not obviously be
180 assigned to either forsterite or enstatite.

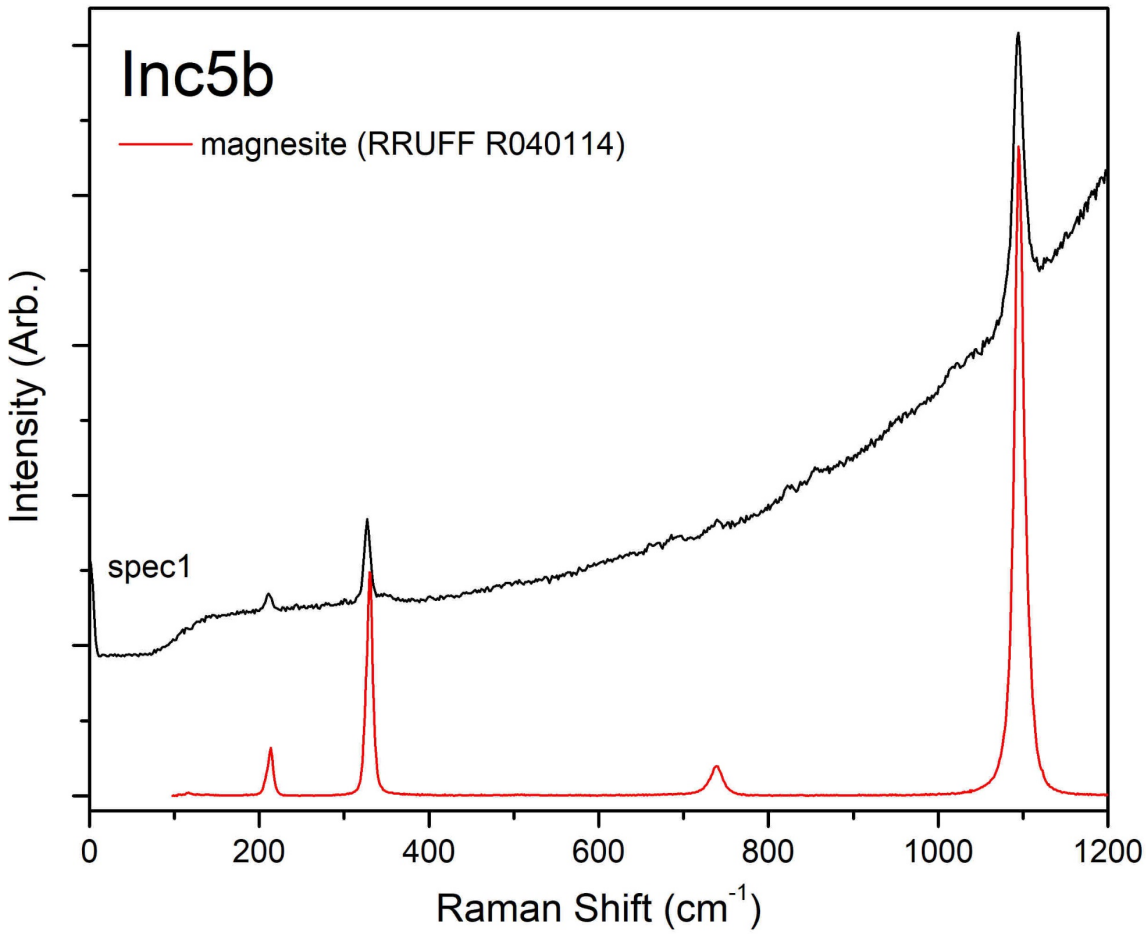


**Supplementary Database 13**: Raman spectra collected at Northwestern University on inclusion 5b showing the presence of magnesite.

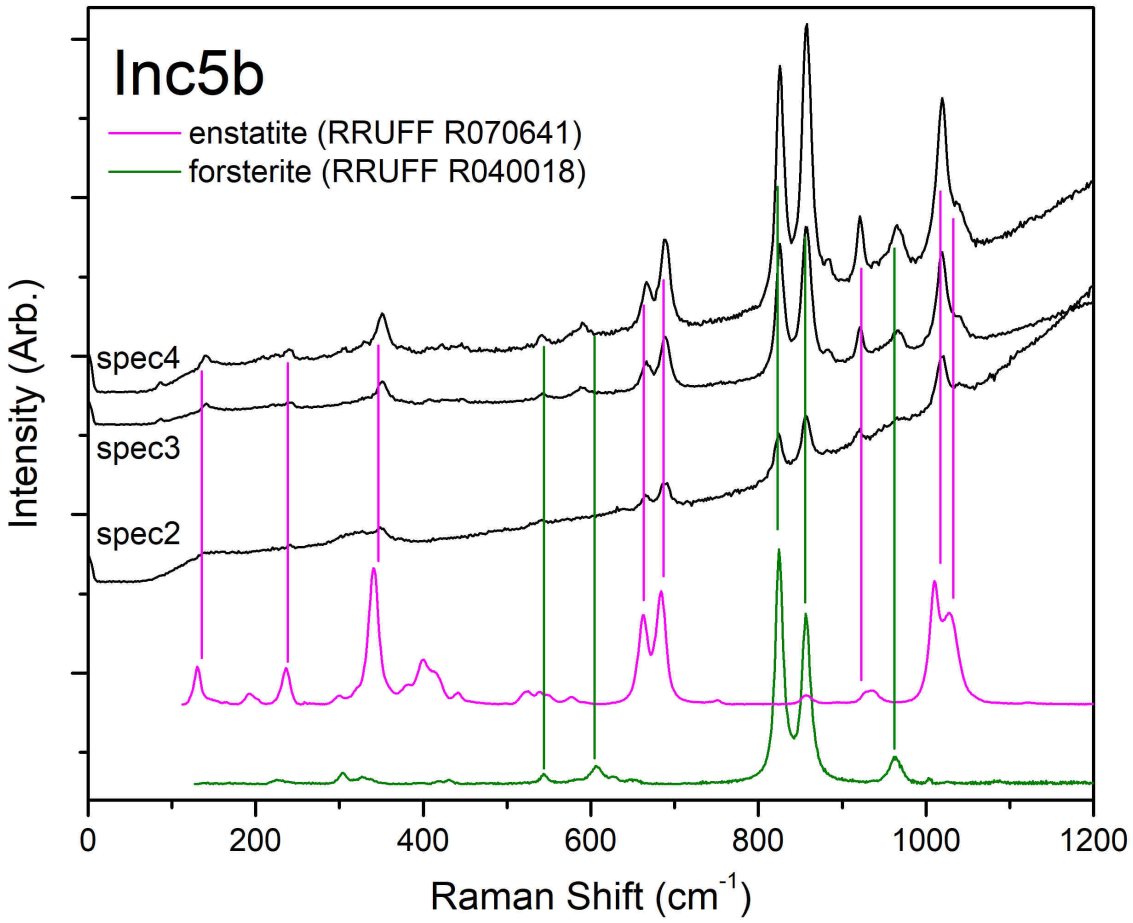


184

185 **Supplementary Database 14**: Raman spectra collected at Northwestern University on inclusion
186 5b showing a mixture of forsterite and enstatite.